Journal of Marine Research, 67, 25–42, 2009

Identification of a cusp catastrophe in a gap-leaping western boundary current

by Joseph J. Kuehl[1,2] and Vitalii A. Sheremet[1]

ABSTRACT

The Luzon Strait is an example of a location where a western boundary current must negotiate a gap in bathymetry. In the gap region, the current can exhibit multiple steady states (leaping the gap or penetrating the gap) and hysteresis (dependence on past flow state). Laboratory experiments on such flows are presented in order to investigate the system behavior in a two-dimensional parameter space of varying flow rate and platform rotation rate. The experiments were performed in a cylindrical tank on a one-meter rotating table. A semi-circular ridge with a gap was inserted over sloping bottom topography in the active region, and the flow was driven by pumping water through sponges. The flow was visualized with the Particle Image Velocimetry method. By varying the flow rate (strength of current), we were able to identify transitions between leaping and penetrating flow states. These transitions bound a region of multiple steady states where hysteresis is present. The dynamics of the system is shown to exhibit a cusp catastrophe classified as A_3. The scaling dependencies of some critical properties of the flow are analyzed.

1. Introduction

The western boundary current Kuroshio, when flowing from the island of Luzon to Taiwan, must negotiate the Luzon Strait. A recent summary of satellite imagery (Caruso *et al.*, 2006) identified several dominant paths the Kuroshio assumes when crossing the strait: a path in which the Kuroshio leaps directly from Luzon to Taiwan; a path in which the Kuroshio bifurcates south of Taiwan with one branch penetrating into the South China Sea and the other continuing north past Taiwan, and several paths in which the Kuroshio penetrates into the South China Sea, forming a loop current, before continuing north. Transitions between these states are irregular and difficult to predict. Caruso *et al.* (2006) cited several different explanations for the transitions. Farris and Wimbush (1996) demonstrated that the local wind stress associated with the strong northeast monsoons and the wind stress history could be responsible for the transitions. In a numerical study, Metzger and Hurlburt (2001) concluded that the flow is nondeterministic as a result of mesoscale flow instabilities caused by eddies and Rossby waves arriving from the western Pacific. A theoretical study

1. Graduate School of Oceanography, University of Rhode Island, 215 South Ferry Road, Narragansett, Rhode Island, 02882, U.S.A.
2. Corresponding author. ***email: jkuehl@gso.uri.edu***

(Sheremet, 2001) and an experimental study (Sheremet and Kuehl, 2007) suggested that the mechanism for transitions is an interplay between the inertia of the current and the planetary β-effect. The last two studies have shown that the flow will transition from gap-leaping to gap-penetrating and back again as the strength of the current is varied. Furthermore, the transition from leaping to penetrating and the transition from penetrating to leaping do not occur at the same current strength. This behavior is known as a hysteresis: the state of the system not only depends on the present parameters, but also on the evolution or history of the system. Yaremchuk and Qu (2004, see their Figure 14) calculated that the Kuroshio transport varies seasonally from approximately 31 Sv in March-April to approximately 24 Sv in October-November and suggested that the lower transport values correspond to the Kuroshio intrusions into the South China Sea, thus confirming the results of Sheremet (2001).

In the present work, we extend the laboratory experiments of Sheremet and Kuehl (2007), which demonstrated the existence of hysteresis, and explore the system's behavior in the two-parameter space of the flow rate and the platform rotation rate. In doing so, we are able to identify and trace a cusp catastrophe surface leading to the existence of multiple steady states and hysteresis. We also employ a modern flow visualization technique: particle image velocimetry (PIV) which allows us to record and analyze various features of the flow associated with transitions between the different flow patterns.

2. Methods

a. Laboratory experiment setup

The laboratory apparatus is similar to that of Sheremet and Kuehl (2007) with a new feature being the PIV system mounted on the platform for flow visualization (Fig. 1). The setup consists of a cylindrical tank of radius $R = 48.7$ cm on a one-meter turn table rotating with angular velocity Ω. The tank is divided in half by a sponge barrier which separates the active region from the forcing region. The active region contains a bottom with slope $S = 0.05$ to simulate the β-effect. North indicates the shallow end, south the deep end, the active region is west, and the forcing region is east. A thin, vertical, impermeable ridge runs from the north pole to the south pole extending $\frac{2}{3}R$ into the active region in a circular arc. The ridge contains a gap of width $2a = 14$ cm at its center. The forcing region is divided into two equal basins, northern and southern. The forcing is achieved by pumping water with volume flow rate Q from the southern basin to the northern basin. The water then percolates through the northern sponge, providing a broad Sverdrup interior circulation. This interior circulation flows along geostrophic contours until it impinges on the ridge, where a boundary current is formed. The boundary current must then negotiate the gap, before being sucked through the southern sponge. The tank is filled with $H_0 = 10$ cm of water, which is measured at the center at rest and has a free surface. Thus the total depth is

$$H(x, y) = H_0 - Sy + \frac{1}{2}\frac{\Omega^2}{g}\left(r^2 - \frac{1}{2}R^2\right) \tag{1}$$

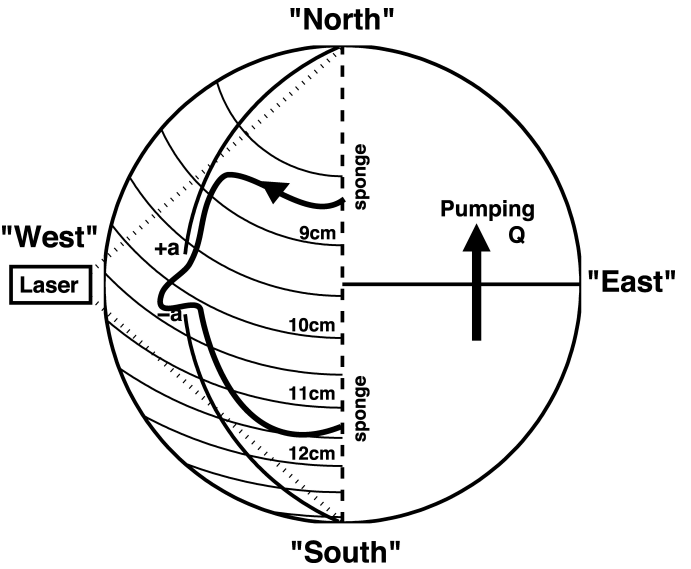

Figure 1. Sketch of the laboratory experiment. The barrier is the great circle interrupted by the gap from −a to +a and in the active region the geostrophic contours (or constant depth contours for solid body rotation) are shown by thin circular lines. The dotted lines from the laser indicate the width of the laser sheet and the camera is suspended directly over the gap.

where $r = (x^2 + y^2)^{1/2}$ is the radius and $g = 980$ cm s^{-2} is the acceleration due to gravity. Because the geostrophic contours (isolines of fluid depth) bend northward, (Fig. 1) due to the paraboloidal shape of the free surface, in our laboratory experiments we generated a boundary current flowing from north to south in order to take advantage of a longer boundary run. This is opposite to the oceanographic case, but according to the quasi-geostrophic approximation north and south directions can be flipped on the β-plane.

For some preliminary experiments, we used dye release visualization with dye being pumped through a needle inserted near the northern end of the tank in such a way that a single dye streak entered the core of the boundary current. However, in the main series of experiments, a LaVision PIV system was used to obtain high-resolution velocity vector fields for quantitative analysis. Our PIV system works as follows. A (50 mJ) Nd-YAG laser fires a (5 ns) pulse of light through a diverging lens which converts the pulse into a horizontal sheet of light illuminating passive seed particles (10 micron in diameter glass spheres) in the fluid. The reflections are imaged by a 1376 × 1040 pixel CCD camera. The laser and camera are synchronized such that each laser pulse corresponds to one image and the time difference (90000 μs) between two consecutive pulses (images) is known. Our system has a maximum frequency of 4 Hz. That is, four two-image pairs may be obtained every second. These setting are adequate for current velocities of a few cm s^{-1}. Once the images are recorded, software correlates the reflection patterns between two consecutive

images splitting them into smaller interrogation windows (32 × 32 pixels) which yields a two dimensional array of velocity vectors. The laser and camera were attached to a superstructure, which was mounted around the tank, on the rotating table. The laser was mounted to the west of the tank and illuminated the gap in a horizontal plane 5 cm above the sloping bottom measured from the center. The camera was suspended directly above the gap.

b. Procedure

Water was stored in open containers over night in order to equilibrate with room temperature. After filling the tank, the temperature was recorded which was usually about 20°C. The tank was then spun up and the flow was allowed to reach solid body rotation. The pumping was then turned on and slowly increased to the desired flow rate. Five to ten minutes were allowed for the flow to reach a steady state. Then it was visualized with either dye injection or a series of PIV images (no less than 60 images taken at 4 Hz). The flow (pumping) rate Q was then increased by 1.66 $cm^3\ s^{-1}$, allowed to reach steady state and imaged again. This process was continued until the flow transitioned from penetrating to leaping. Then the process was reversed, with the flow rate being decreased by 1.66 $cm^3\ s^{-1}$ in each step, until the flow transitioned back to the penetrating pattern. This constituted one experiment. Several experiments were run at different table rotation rates. The critical flow rates at which the flow transitions are of particular interest.

3. Cusp catastrophe surface

The product of one experiment was a time series of vector velocity fields for different flow rates (Fig. 2). It is convenient to characterize the state of the system by a single value as opposed to an entire vector field. From many possible options, we have chosen the position of maximum southward velocity along an east-west section passing through the gap. This position identifies the location of the core of the current. The particular section chosen lies 1/4 gap width or 3.5 cm to the south of the center line and captures the most variation of the flow pattern. In this way, a given experiment may easily be summarized by a single plot in which east-west position of maximum southward velocity is plotted against flow rate (Fig. 3). Larger values of maximum velocity position correspond to the jet penetrating farther into the gap, up to the limiting position at the edge of the tank at 48.7 cm. On the other hand, the gap leaping state is characterized by the position near the gap center at 32.5 cm. The arrows indicate the sense in which the flow states are traversed as an experiment proceeds. The error bars represent one standard deviation calculated from a time series of at least 60 vector fields taken at 4 Hz. Only the position of maximum velocity was plotted. We did not account for the breadth of the flow. However, the trends in the data are apparent. As the flow rate was increased, we see the flow transition from a penetrating state to a leaping state. As the flow rate was decreased, we see the flow transition back. However, the location of the transitions are not the same for increasing and decreasing flow rates. These figures are, in

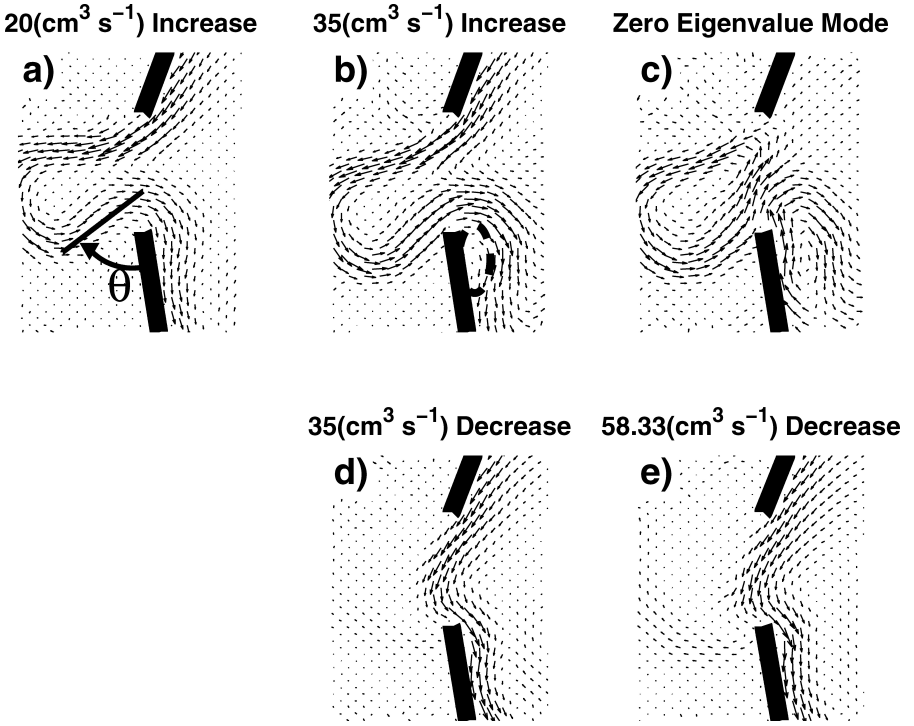

Figure 2. Examples of averaged velocity vector fields obtained with the PIV system for different flow rates and fixed rotation rate 1 rad s^{-1}. The thick black lines mask the edges of the gap. The current flows from top (north) to bottom (south). The upper panels (a) and (b) correspond to increasing flow rate, while the lower panels (d) and (e) correspond to decreasing flow rate. Different steady states are apparent for a flow rate of 35 cm^3 s^{-1} (b) and (d). The panel (c) represents an approximation to the zero eigenvalue mode (explained at the end of Section 3) giving rise to multiple states and is a difference between the vector fields (b) and (d). The small dashed semicircle in (b) highlights a recirculation gyre which is present for certain parameter values, and angle θ is shown.

fact, classic hysteresis curves (Gilmore, 1981, Chap. 9). Where the two tracks (increasing and decreasing) do not overlap, the flow exhibits multiple steady states, at least three: two indicated in the figure and one implied (see below). That is, for the same parameter values, the system may have more than one steady state. Which state is realized depends on the prior state of the flow, in other words, the system displays hysteresis.

The region of multiple steady states and hysteresis is bounded by the transitions between leaping and penetrating flow states. When hysteresis curves for different rotation rates are compared, we notice the region of multiple steady states is larger and more distinct for high rotation rates than for low rotation rates. In fact, for low enough rotation rates ($<$0.40 rad s^{-1}), hysteresis is no longer present. The flow transitions smoothly and monotonically from leaping to penetrating and back along the same path.

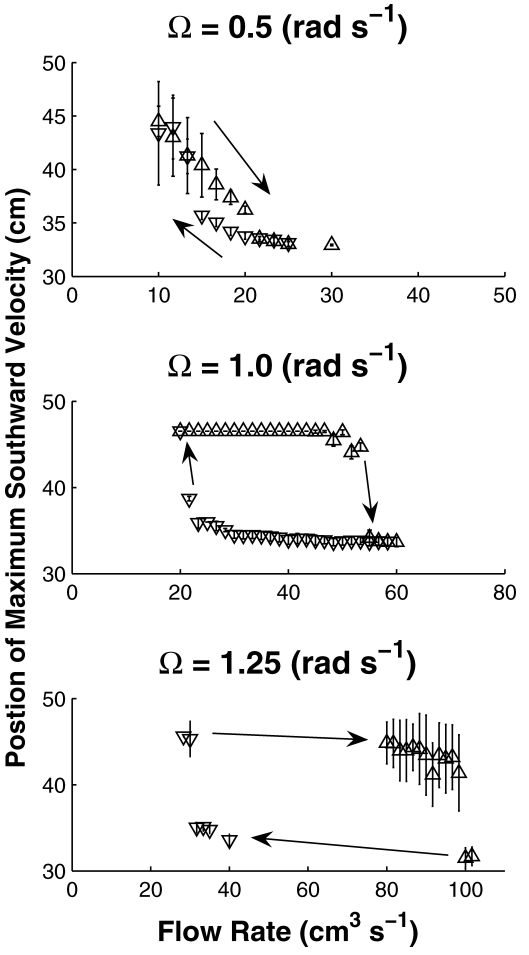

Figure 3. Three hysteresis curves are shown for rotation rates of 0.5 rad s^{-1}, 1.0 rad s^{-1}, 1.25 rad s^{-1}. Position of maximum southward velocity (larger values correspond to penetrating flow states) is plotted against flow rate. The velocity is measured along an east-west section passing 3.5 cm south of the center of the gap. Upward pointing triangles represent flow states with increasing flow rate steps, and downward pointing triangles indicate decreasing flow rate steps. The arrows indicate the sense in which the hysteresis curves are traversed as an experiment proceeds. Error bars represent one standard deviation.

The hysteresis curves considered together in the two-parameter space of flow rate Q and rotation rate Ω define a surface on which the state of the system is confined (Fig. 4). The upper surface corresponds to the stable penetrating states. If the flow is in one of these states and the system parameters are varied (say flow rate is increased), the system moves along this surface. As the parameter moves beyond the "fold," the system "falls off the

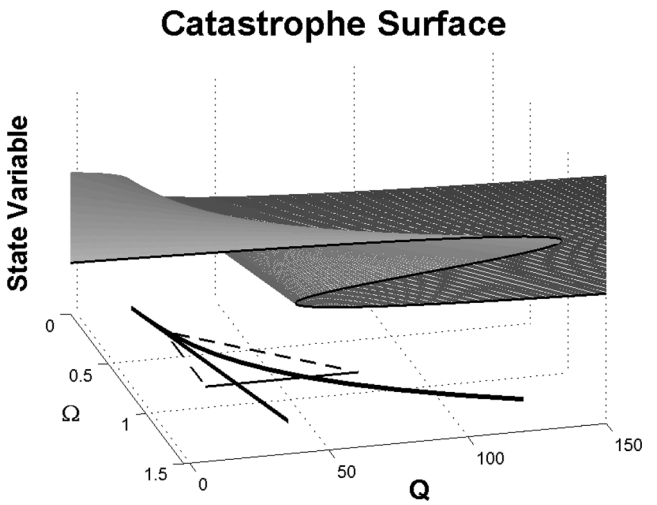

Figure 4. An illustration of a cusp catastrophe surface. The surface was fit to our experimentally determined bifurcation set (Fig. 5). Thus, it accurately approximates the systems transitions. The surface represents a manifold on which the state of the system is confined. The interesting dynamics occur in the region where the surface folds over on itself. The z axis represents the state parameter: the position of the maximum southward velocity (Fig. 3). The larger values correspond to penetrating states and smaller values to leaping states. The edges (folds) correspond to the parameters at which transitions occur. The projection of the edges onto the parameter space is the bifurcation set, shown by the black 'v' shape. The bifurcation set divides the parameter space into distinct region. The solid line represents a system evolution path in which a rapid transition occurs. The dashed lines represent a system evolution path in which the bifurcation set is avoided and the system evolves without a rapid transition.

edge," jumping down to the lower surface. This jump is the transition from penetrating to leaping. Now the system is confined to the lower surface, which corresponds to stable leaping states. The system will remain on this lower surface until the parameters are varied in such a way that a second set of critical parameters is crossed (the lower "fold"). When this happens, the system jumps up to the upper surface. This jump is the transition from leaping to penetrating. Note that the transition from one state to another has nothing to do with an instability to small-scale perturbations but rather with the disappearance or turning of a particular branch of steady solution. In the language of mathematics it is a catastrophe: small changes in control parameters move the system over the edge and cause large change (jump) in the system state. The parameters may be varied in such a way that the system moves around, avoiding, the folds and transitions smoothly between states (dashed lines in Fig. 4). The surface on which the state of the system is confined is known as the catastrophe surface. The topology when two folds merge is classified as a cusp catastrophe of type A_3 (Gilmore, 1981, Chap. 6). The folds, where transitions occur, when projected onto the parameter space, are known as the bifurcation set (the 'v' shaped projection in Fig. 4) which

divides the parameter space into regions where one or three (possibly more) states exist. We notice that the interesting dynamics occur when the surface wraps around on itself.

It is worth mentioning the meaning of the middle surface. While the upper and lower surfaces represent stable penetrating and leaping states respectively, the middle surface represents an unstable state, hence it cannot be detected experimentally. According to the bifurcation theory, there is usually a non-oscillatory eigenmode associated with such instability. On the lower and upper surfaces this eigenmode is decaying, while on the middle branch it is amplifying. At the folds the eigenvalue of this mode vanishes. The spatial pattern of this eigenmode can be approximated by taking a difference between the flow patterns at the upper and lower branches which is shown in Figure 2c. Another geophysical example of multiple steady states and calculation of true eigenmodes in the context of a recirculation gyre can be found in Sheremet *et al.* (1997).

We stress that the choice of a particular state variable to describe the flow patterns (be that the position of velocity maximum, a characteristic stream line, or something else) does not affect the transition points. The state variable as a function of the control parameter is *multivalued* and has an S-shaped form (with the middle branch unrealizable). At the critical or transition points the derivatives are infinite and clearly they are infinite for any choice of the state variable.

Plotting the location of flow transitions from our experimental data, we are able to identify the bifurcation set of our system (Fig. 5). The upper curve corresponds to the parameter values at which the system transitions from penetrating to leaping and the lower curve corresponds to parameter values at which the system transitions from leaping to penetrating. The intersection of the two curves corresponds to a cusp singularity: a point where two folds coalesce. The bifurcation set bounds the region of multiple steady states and hysteresis (Region 3). Region 2 corresponds to penetrating flow only. Region 4 corresponds to leaping flow only. In Region 1, hysteresis is not present and the system evolves from one state to the next smoothly. The cubic and linear fit are consistent with scaling arguments (below).

4. Quantitative results

Because of the rapid rotation, the flow, to large degree, can be described by the quasi-geostrophic potential vorticity advection-diffusion equation written in terms of the stream function $\psi(x, y)$

$$J(\psi, \nabla^2\psi) + \beta\psi_x = -r\nabla^2\psi + \nu\nabla^4\psi \tag{2}$$

where J is the Jacobian operator; $\beta = 2\Omega S/H_0$ is the topographic β-effect; $r = \Omega h_E/H_0$ is the bottom drag; $h_E = \sqrt{\nu/\Omega}$ is the Ekman thickness; ν is the fluid viscosity. Three boundary layer length scales are commonly associated with (2): $L_I = \sqrt{U/\beta}$ is the inertial boundary layer thickness, $U = Q/(H_0 R)$; $L_S = r/\beta$ is the Stommel boundary layer thickness due to bottom drag; and $L_M = (\nu/\beta)^{1/3}$ is the Munk boundary layer thickness due to lateral viscosity. In varying the platform rotation Ω all three scales were affected through the β-effect, while in varying the pumping rate Q only L_I is changed. In our laboratory

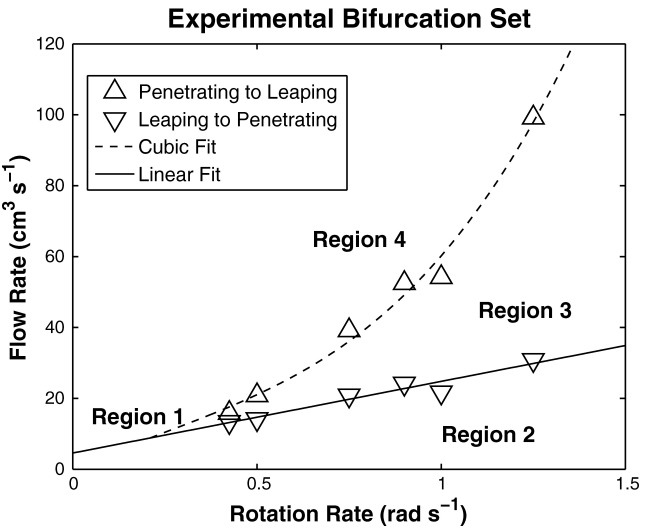

Figure 5. Experimentally determined bifurcation set of the system. Upward pointing triangles represent parameters at which the system transitions from penetrating to leaping. Downward pointing triangles represent parameters at which the flow transitions from leaping to penetrating. Region 4 corresponds to leaping states only. Region 2 corresponds to penetrating states only. Region 3 is the region of multiple steady states and hysteresis. In Region 1, hysteresis is no longer present. The cubic and linear fits shown are consistent with scaling arguments (below).

experiments all three scales L_I, L_S, and L_M were of the same order of magnitude with L_I dominating for larger flow rates. A combination of these length scales determines the scale of the boundary current L_B, and hence, the magnitude and shape of the boundary velocity profile upstream of the gap, which is central to understanding the dynamics of the system. The definition and quantitative derivation of L_B can be found in the Appendix. The quasi-geostrophic assumption holds very well in the Sverdrup interior, but it is not very accurate in the western boundary current, where the relative vorticity can be comparable with the Coriolis parameter, especially in the viscous sublayer. Nonetheless, (2) holds due to the two-dimensional character of the flow there and relatively small change of the fluid depth.

Examples of the velocity profiles for varying flow rates ($Q = 10$, 20, and 30 cm^3 s^{-1}) and rotation rates ($\Omega = 0.5$, 0.75, and 1.25 rad s^{-1}) are shown in Figure 6. The profiles are taken slightly upstream of the northern edge of the gap perpendicular to the boundary. We see that the profiles are roughly exponential except for a narrow viscous sublayer near the wall. We also see that the numerical and analytical models represent the experimental data very well. A small discrepancy can be noticed, however, in the outer boundary layer structure for large Ω. The reason is that for $\Omega > \sqrt{gS/R} = 1$ rad s^{-1} the slope of the parabolic free surface in the source region exceeds the slope of the bottom S which results

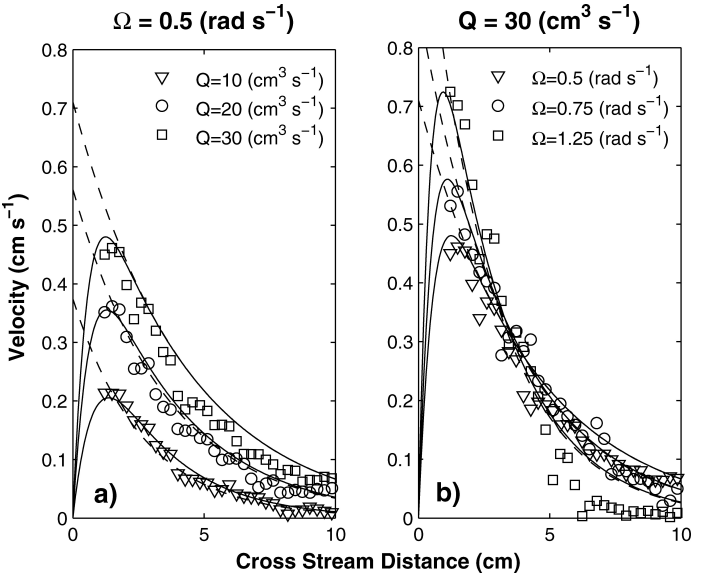

Figure 6. Velocity profile comparison between model and experiment: (a) for varying flow rate Q; (b) for varying rotation rate Ω. The experimental velocity profiles based on PIV data are shown by symbols. The numerical solution of one-dimensional boundary layer equation (8) is shown by solid lines while the analytic approximation according to (10) is shown by dashed lines. Dips near 2 and 4 cm in the PIV data are due to shadows and reflections in the tank that could not be removed.

in formation of closed geostrophic contours there and somewhat alters the structure of the Sverdrupian flow outside the western boundary current. Though the PIV method does not allow us to resolve the viscous sublayer completely (the enhanced laser reflections from the ridge require masking in that region), the maximum velocity of the boundary current can still be obtained quite reliably by combining laboratory and numerical results. This is due to the fact that the one dimensional numerical model (in which molecular viscosity is assumed) is in good agreement with the PIV data over most of the boundary layer and the fact that the maximum velocity is restricted by the total transport in the boundary layer, most of which is well resolved.

A scaling analysis was used in Sheremet (2001) to predict the asymptotic shape of the bifurcation set in the case of exactly parallel western boundary flow of Munk thickness, $L_B = L_M$. The method is based on the assumption that the respective flow pattern breaks down and transition occurs when the nonlinear terms in (2) become comparable with other terms. The breakdown of the penetrating state (β-plume) is predicted by balancing the zonal advection with the β-effect, while for the breakdown of the gap leaping state the meridional advection has to be balanced with the β-effect. This results in different scaling behavior and divergence of the bifurcation set branches as the gap width is increased.

In the present case the boundary layer thickness is dominated by the inertial scale, $L_B \simeq L_I$. Also the gap width was fixed here, but the rotation rate of the platform was varied instead. Nonetheless, as Figure 5 shows, the bifurcation set branches do diverge as well. This is a universal character of a cusp catastrophe surface: in the vicinity of the cusp point any two governing parameters would reveal the same topological structure with diverging branches.

With the present laboratory setup, we cannot recover the asymptotic behavior of the gap penetrating flow pattern because of the limited extent of the region west of the gap. However, the gap leaping flow pattern appears to exhibit a clear scaling which is analyzed below. When lateral and bottom friction are small compared to advection, which is true if $L_S, L_M \ll L_I$, we can assume that the current, as it leaves the boundary and enters the gap region, approximately conserves potential vorticity following the streamline. This assumption is supported by the observation that the core of the jet approximately follows a line of constant potential vorticity (Fig. 7, right panel)

$$\frac{2\Omega + \zeta_0}{h_0} = \frac{2\Omega + \frac{dV}{dn} - KV}{h_0 - S(y - y_0)} \tag{3}$$

where we have expressed relative vorticity in terms of cross stream shear, velocity magnitude V, and curvature K; the subscript 0 indicates quantities evaluated in the boundary current just upstream of the separation point, and the left-hand side of (3) is the initial potential vorticity. The above assumption is further supported by the observation that the cross stream structure of the current remains fairly constant as the jet crosses the gap. For three cross sections taken as the jet leaps across the gap (Fig. 7, left panel), we identify the position of maximum velocity as well as the positions of half maximum velocity on both sides of the jet. The distances between the maximum and the half maximum velocities are calculated. The ratio of these two distances provides a proxy for the structure of the jet. A large or small ratio, compared to one, indicates a highly asymmetric jet. The ratios for the three section are: A = 0.59, B = 0.60, C = 0.60. This lends support for our assumption that the structure of the jet does not vary significantly as the jet leaps the gap. By choosing to trace a streamline which corresponds to the maximum velocity of the current, the existence of which is suggested by the knowledge that the cross stream structure of the jet does not vary significantly, we are able to set $\frac{dV}{dn} \approx 0$ and $\zeta_0 \approx 0$ and solve for K.

$$K = \frac{2\Omega S(y - y_0)}{h_0 V} = \frac{1}{R_c}, \tag{4}$$

where R_c is the local radius of curvature. Note that for large V or small Ω we expect large R_c meaning that the current will flow straight across the gap. For small V or large Ω the curvature is significant. Physically the curvature of the current is balancing the topographic β-effect. For large flow rates the curvature is small. However, as the flow rate is decreased, the curvature must increase to compensate. If the flow rate is diminished too much, the

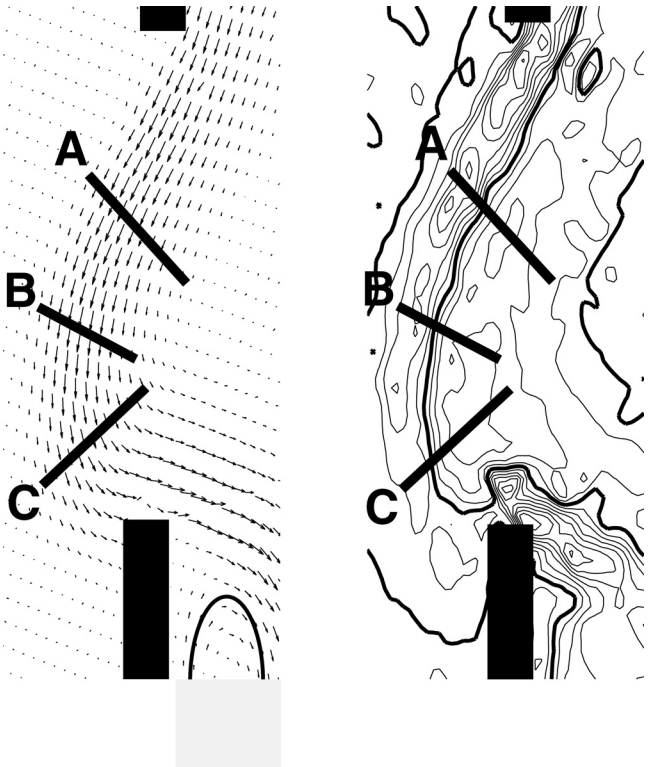

Figure 7. These plots are zoomed in on the gap region. Left Panel: PIV vector field of the flow for $\Omega = 1.0\,\mathrm{rad\,s^{-1}}, \mathrm{Q} = 23.33\,\mathrm{cm^3\,s^{-1}}$ (just before transition). The black lines represent approximate positions of three sections taken across the jet as it leaps the gap. These sections are used to verify that the structure of the jet does not vary significantly as the jet leaps the gap. The half ellipse highlights a recirculation gyre present for certain parameter values. Right Panel: Contour levels of potential vorticity calculated from the flow pattern in the left panel. The bold curve indicates the fH_0^{-1} level. Level intervals are every $0.05\,fH_0^{-1}$. Notice that the core of the jet approximately follows a line of constant potential vorticity.

curvature will become too large and the flow will wrap around on itself. Thus an eddy will form, which will travel westward under the influence of the β-effect, and the flow will transition from leaping to penetrating.

We propose that the transition from a gap leaping current to a gap penetrating current will occur when the following critical condition is satisfied: the radius of curvature (4), evaluated in the middle of the gap ($y_0 - y = a$) and thus the radius of the newly formed eddy, will be equal to the half width of the gap a. Expressed in terms of the maximum current velocity V_m upstream of the gap, this condition (4) is

$$V_m = \frac{2S\Omega a^2}{h_0} = \beta a^2 \tag{5}$$

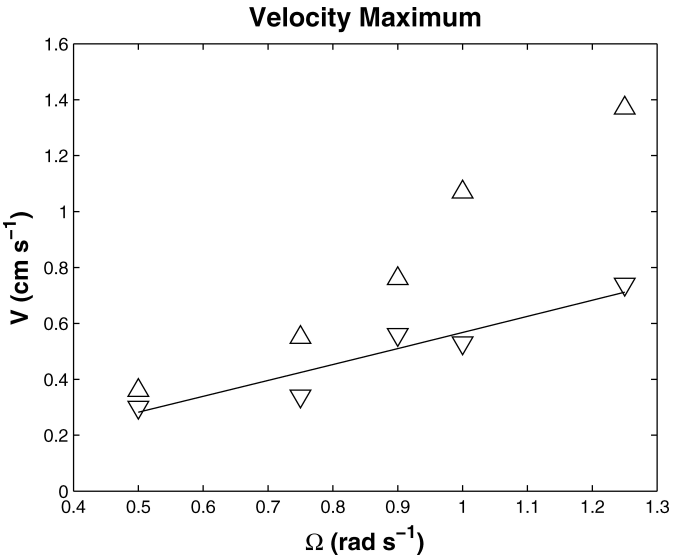

Figure 8. The dependence of the critical maximum boundary current velocity V_m slightly upstream of the gap on the rotation rate Ω based on the PIV derived data. The upward pointing triangles indicate penetrating to leaping transition as Q is increased. The downward pointing triangles indicate leaping to penetrating transition as Q is decreased. The straight solid line shows the linear theoretical scaling based on (5).

where the local depth h_0 is very close to H_0 because, at the position of the gap, the contribution of the free surface paraboloid to the total depth almost vanishes (1).

Based on the PIV data combined with the one dimensional numerical model, we determined the critical maximum boundary current velocity V_m slightly upstream of the gap for critical parameters along the bifurcation set (Fig. 8). The transition from penetrating to leaping for increasing Q is indicated by upward pointing triangles (the upper branch), while the transition from leaping to penetrating for decreasing Q is indicated by downward pointing triangles (the lower branch). The theoretical scaling based on (5) representing the linear dependence on Ω is marked by the straight line and is in a good agreement with the experimental data for this branch.

Because the velocity profile is approximately exponential (Fig. 6) the pumping rate Q is related to V approximately according to

$$Q \simeq V L_B H_0, \tag{6}$$

where $L_B = L_I = \sqrt{Q/(H_0 R\beta)}$ is dominated by the inertial boundary layer thickness which in turn depends on Q. Thus in terms of the pumping rate, the critical condition can be written as

$$Q \simeq \frac{\beta a^4 H_0}{R} = \frac{2\Omega S a^4}{R}, \tag{7}$$

exhibiting a linear behavior with Ω as well, which was shown in Figure 5 by a solid straight line.

5. Leading edge recirculation eddy

Another interesting phenomenon captured by the laboratory experiments is the formation of a recirculation eddy near the tip of the ridge as the loop current exits the marginal sea. It has an analogy with leading edge separation of flow around a flat plate. In the ocean this feature is observed east of the southern tip of Taiwan (Chunsheng and Li, 2003) and next to the Island of Lanyu; therefore it is called the Lanyu Eddy. This recirculation eddy has the potential to create significant upwelling and is important for local fisheries.

In order to analyze the behavior of the the recirculation eddy in the laboratory experiments we introduce two quantities. The size of the eddy b is measured in the direction perpendicular to ridge wall. The eddy itself has approximately an elliptical shape as illustrated in Figure 7 and it is bound by the streamline that separates from the tip of the ridge. Another relevant quantity is the angle θ of the jet before it exits the gap as illustrated in Figure 2a. The angle is 90° when the jet is normal to the wall and decreases as the jet loops farther to the south on the west side of the gap. We plot b (circles) and θ (squares) in Figure 9 as a function of transport Q in a typical experiment with fixed $\Omega = 1$ rad s^{-1}. The open markers correspond to the gap-penetrating branch of flow patterns while closed ones correspond to the gap-leaping pattern. It is evident in the laboratory experiment, that the recirculation eddy is most dramatic as the bifurcation set (system transition) is approached: the eddy size b is maximal at $Q = 53$ cm^3 s^{-1} for gap-penetrating branch and $Q = 22$ cm^3 s^{-1} for gap-leaping branch i.e. just before transitions occur. For the penetrating to leaping state the size of the recirculation eddy seems to grow as the square root of the flow rate above some critical value ($b = A\sqrt{Q - Q_c}$) (Fig. 9). This is consistent with a general observation that the recirculation eddies in flow past solid bodies grow linearly with the Reynolds number or flow velocity (Batchelor, 2000, Chap. 4.12). Due to a predominantly inertial character of the boundary layer in our case, the typical velocity V is proportional to $Q^{1/2}$. We also stress that the large recirculation eddy is only present near the transitions between the states. In that case, the angle the jet makes with the southern edge of the gap wall, as it loops into the gap and flows out around the southern edge, appears to depend linearly on the flow rate. The eddy is not detected for rotation rates of 0.5 rad s^{-1} and lower.

6. Discussion

Our laboratory model is a very idealized representation the Kuroshio current in Luzon Strait area. It lacks, of course, a lot of aspects such as realistic bathymetry, stratification, mesoscale disturbances coming from the Pacific ocean, etc. However, the main similarity is that a predominantly inertial western boundary current, supported by a vertical wall, on a β-plane, which encounters a gap, can exhibit distinct multiple flow patterns.

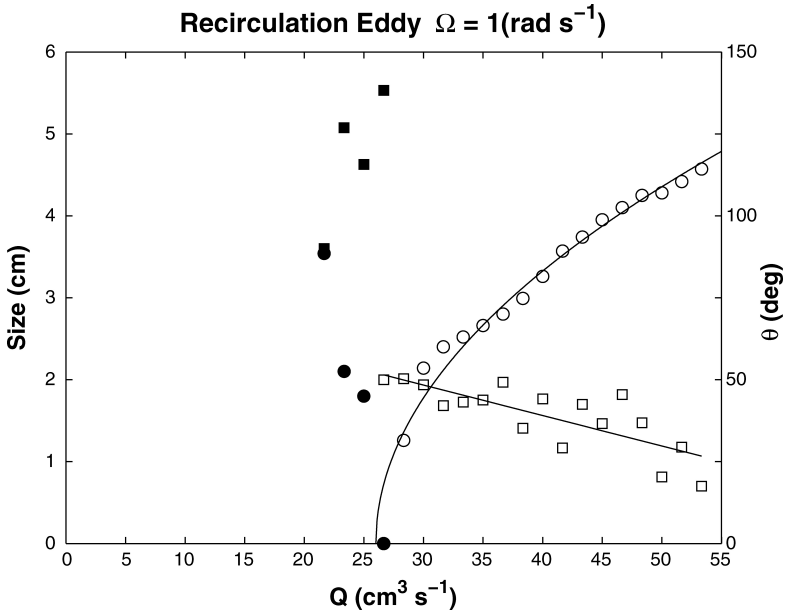

Figure 9. Size of the recirculation eddy *b* measured perpendicular to the ridge wall and angle θ the current makes with the southern wall before flowing south around the southern gap edge (Fig. 2a). Zero angle corresponds to northward flow along the wall towards the gap, which then wraps around the gap edge and continues south. 90° is flow impinging normally on the southern gap wall from the west. Squares indicate angles, circles indicate size *b*. Open symbols correspond to penetrating flow states before the transition, and filled symbols correspond to leaping flow states just before the transition. A square root and linear fit are shown for radii and angle, respectively, for penetrating flow states.

Our north-to-south flipping in the laboratory setup is dictated by desire to change the shape of the geostrophic contours in the Sverdrup interior where the quasi-geostrophic approximation is justified by smallness of the Rossby number of the mean circulation which is true both in the ocean and in the laboratory. The quasi-geostrophy is not very accurate in the western boundary currents where relative vorticity may be comparable with the Coriolis parameter. This is a consequence of the potential vorticity conservation in a predominantly inviscid flow. A more appropriate approximation in that case is a semi-geostrophy: the geostrophic balance is applied only across the stream, while along the stream the inertial effects must be taken into account. Both the velocity profiles (Fig. 6) and potential vorticity field (Fig. 7, Right Panel) show the relative vorticity as large as 0.6Ω especially in the viscous sublayer. The inertial nature of the western boundary currents has been observed and recognized a long time ago in application to the Gulf Stream (Stommel, 1965) and Kuroshio (Stommel and Yoshida, 1972, Chap. 5). Similar to the oceanic case our laboratory boundary current is dominated by inertia which is manifested by the exponential velocity profile of an accelerating boundary layer.

We have shown the existence of a cusp catastrophe in such a system. The bifurcation set associated with this catastrophe gives the location of transitions between leaping and penetrating states, and bounds the region of multiple steady states and hysteresis. The identification of this catastrophe must be considered in theoretical and observational analysis of gap leaping flows. The main implication is that when analyzing observational data a simple linear correlation between the state of the system and values of external parameters may not be adequate to properly describe such relationships: the prior evolution and hysteresis should be taken into account.

In the laboratory experiments, we explored the system in a two-dimensional parameter space of varying the flow rate and rotation rate. While the former has a direct oceanic analogy, the western boundary current transport or its inertia, the later has only an indirect analogy. According to Farris and Wimbush (1996) the local wind stress associated with the Northeast monsoon has a significant effect on the pathway of the Kuroshio in Luzon Strait. Though the wind-driven Ekman transport is small to account for the possible Kuroshio inflow through the strait, it may accomplish this by slightly steering the axis of the current. In the laboratory as the rotation rate Ω is varied, the angle at which the geostrophic contours strike the ridge changes. For small Ω they are normal to the ridge, for larger Ω as the parabolic shape of the free surface is increased according to (1), the geostrophic contours bend towards north. That effectively changes the angle of the boundary current relative to geostrophic contours within the gap region.

The limited extend of our tank west of the gap has certain implications. While the edge of the tank is clearly unlikely to have much effect on the transition from a jet leaping the gap to one penetrating into the gap, we anticipate that the opposite transition is likely to be affected, but not significatly. This is because just before the critical situation is reached the loop current shrinks and does not touch the western wall. Another aspect is that the distance between the gap and outer tank wall is approximately the gap width ($2a$) and is also the length scale for eddies that could form in this system. The system is thus forced to a steady state by interactions with the outer wall, instead of the eddy shedding state observed by Sheremet (2001). Additional laboratory experiments, that we conducted in a different tank with a larger gap-to-western-wall distance, showed that the stable penetrating state is replaced by a nearly periodic eddy shedding state. The multiple steady states, hysteresis, and cusp catastrophe are all retained in the system's dynamics. The steady state situation presented here is beneficial in that the underlying dynamics of the system is more transparent, lacking the complicated eddy stresses.

Thus, the cusp catastrophe reported here may be a useful guide in analyzing the dynamics of the real ocean and those simulated by numerical ocean models. In particular, it was observed in the laboratory that an eddy pinch off occurred whenever the flow transitioned along a trajectory which crossed the bifurcation set. This suggests a different eddy shedding mechanism in addition to a periodic eddy shedding state. This mechanism is similar to the eddy shedding occuring seasonally due to transformation of mean circulation in Luzon Strait recently reported by Yuan *et al.* (2007).

Acknowledgments. This work was supported by the National Science Foundation Grant OCE-0351518, and ONR Grant N000140210271. The authors are also thankful to Dr. Mark Wimbush for many helpful comments and suggestions, Dr. Peter Cornillon for maintaining the GSO/GFD laboratory and assisting our research project, as well as two anonymous reviewers.

APPENDIX

One-dimensional accelerating boundary layer model

The scaling analysis employed to predict the transition from leaping to penetrating states depends on the boundary layer length scale. To determine it we consider an idealized situation where a uniform westward zonal flow with velocity U impinges normally on a straight meridional boundary. Due to symmetry, the stream function can be sought in the form $\psi(x, y) = UyF(x)$, where F is the non-dimensional structure function. Here we assume that the boundary current flows northward and y is the distance from the latitude of the current origin. In the case of Kuroshio, the origin is the latitude of the North Equatorial Current bifurcation. In the case of the laboratory experiment, the origin is the tank wall and y is the distance along the inflow sponge. Upon substituting into a governing quasi-geostrophic equation (2) a one-dimensional ordinary differential equation for F is derived

$$L_I^2[F'F'' - FF'''] + F' = -L_S F'' + L_M^3 F^{IV} \tag{8}$$

where L_I, L_S, L_M are the same as introduced in the main text. At the western boundary $x = 0$ the conditions $F(0) = 0$, $F'(0) = 0$ represent no-throughflow and no-slip while the total transport and decay of perturbations conditions $F(\infty) = 1$, $F'(\infty) = 0$ are specified outside the boundary layer, $x \gg L_I, L_S, L_M$.

The nonlinear problem (8) was solved numerically using a simple centered finite difference approximation coupled with a time equilibration method. For typical experimental parameters the velocity profile F' consists of an inertially dominated exponential outer boundary layer and a relatively narrow viscous sublayer near the wall where the velocity vanishes. The outer exponentially decaying tail can be described analytically by

$$F(x) = 1 - exp(-\lambda x) \tag{9}$$

where λ satisfies a cubic

$$L_M^3\lambda^3 - L_I^2\lambda^2 - L_S\lambda + 1 = 0 \tag{10}$$

resulting from (8). Of three possible values, we selected the smallest positive root appropriate to the outer boundary layer region. Based on the exponential decay scale, we define the boundary current width as $L_B = 1/\lambda$ which is a function of the three parameters L_I, L_S, L_M.

REFERENCES

Bakker, P. G. 1991. Bifurcations in Flow Patterns, Kluwer Academic Publishers, 209 pp.

Batchelor, G. K. 2000. An Introduction to Fluid Dynamics, Cambridge Univ. Press, 615 pp.

Caruso, M. J., G. G. Gawarkiewicz and R. C. Beardsley. 2006. Interannual variability of the Kuroshio intrusion in the South China Sea. J. Oceanogr., *62*, 599–575.

Castrigiano, D. and S. Hayes. 2004. Catastrophe Theory, Westview Press, 264 pp.

Chunsheng, J. and L. Li. 2003. An initial note on quasi-stationary, cold-core Lanyu eddies southeast off Taiwan Island. Chinese Science Bulletin, *48* (19), 2101–2107.

Cushman-Roisin, Benoit. 1994. Introduction to Geophysical Fluid Dynamics, Prentice-Hall Inc., 320 pp.

Farris, A. and M. Wimbush. 1996. Wind-induced Kuroshio intrusion into the South China Sea. J. Oceanogr., *52*, 771–784.

Gilmore, Robert. 1981. Catastrophe Theory for Scientist and Engineers, John Wiley and Sons Inc., 666 pp.

Ierley, G. R. and V. A. Sheremet. 1995. Multiple solutions and advection-dominated flows in the wind-driven circulation. Part 1: Slip. J. Mar. Res., *53*, 703–737.

Metzger, E. J. and H. E. Hurlburt. 2001. The nondeterministic nature of Kuroshio penetration and eddy shedding in the South China Sea. J. Phys. Oceanogr., *31*, 1712–1732.

Pedlosky, J. 1987. Geophysical Fluid Dynamics, Springer, 710 pp.

Sheremet, V. A. 2001. Hysteresis of a western boundary current leaping across a gap. J. Phys. Oceanogr., *31*, 1247–1259.

Sheremet, V. A., G. R. Ierley and V. M. Kamenkovich. 1997. Eigenanalysis of the two-dimensional wind-driven ocean circulation problem. J. Mar. Res., *55*, 57–92.

Sheremet, V. A. and J. Kuehl. 2007. Gap leaping western boundary current in a circular tank model. J. Phys. Oceanogr., *37*, 1488–1495.

Stommel, H. 1965. The Gulf Stream: A Physical and Dynamical Description, Cambridge University Press, 248 pp.

Stommel, H. and K. Yoshida, eds. 1972. Kuroshio, Its Physical Aspects, University of Tokyo Press, 517 pp.

Yaremchuk, M. and T. Qu. 2004. Seasonal variability of the large-scale currents near the coast of the Philippines. J. Phys. Oceanogr., *34*, 844–855.

Yuan, D., W. Han, and D. Hu. 2007. Anti-cyclonic eddies northwest of Luzon in summer–fall observed by satellite altimeters. Geophys. Res. Lett., *34*, L13610, doi:10.1029/2007GL029401.

Received: *7 February 2008*; revised: *28 January 2009*.